

Characterization of Dynamic Friction Factor for FEM Modeling of High Speed Process

Jean-Jacques ARNOUX, Guy SUTTER, Gautier LIST

Laboratoire d'Etude des Microstructures et de Mécanique des Matériaux
UMR CNRS 7239- Ile du Saulcy – 57045 Metz cedex
e-mail: {jean-jacques.arnoux,guy.sutter,gautier.list}@univ-lorraine.fr

The present study aims to establish through a series of friction tests the trends of the dynamic factor according to sliding speed. A ballistic set-up using an air gun launch is used to measure the friction coefficient for the steel/carbide contact between 15 m/s and 80 m/s. Since the experimental characterization of friction is a key factor in the development of high speed process such as high speed machining, the experimental quantification is introduced into a cutting model by finite elements method. Modeling results are compared with cutting forces measured on a similar experimental device, which can reproduce perfect orthogonal cutting conditions.

Key words: dynamic friction, ballistic set-up, high speed process, finite element method.

1. INTRODUCTION

The frictional phenomena at the tool-chip interface cause plastic deformations in a region of the chip adjacent to the tool rake face. In this area, called secondary shear zone, the material is subjected to high shear producing an important rise in temperature due to friction and plastic work. Close to the cutting edge, the pressure is very large (~ 1 GPa) and the material speed is severely reduced. The friction stress has a value in the order of the flow stress k in the chip. The pressure progressively decreases by moving away the tool tip, and at the end of the contact, the sliding speed tends to the chip velocity V_{chip} . In this zone, the relationship between the normal stress σ_n and the tangential stress τ_n is usually modeled using the friction Coulomb's law:

$$(1.1) \quad \tau_f = \mu \sigma_n,$$

where μ is the friction coefficient. The friction coefficient μ is therefore representative of the sliding contact for pressures of several hundred MPa. In analytical

and numerical models of metal cutting, the knowledge of the value of μ is very important because it controls both the cutting force and the temperature rise at the contact. To choose the suitable value of μ , experimental results such as those found thanks to “split tool” method [1–3], should be used. Unfortunately, these experiments are still infrequent and reserved for conventional machining (low cutting speed). Moreover, experimental results based on the “split-tool” show a high degree of incertitude in the determination of μ .

An alternative way to select the values of μ is to use other experiments that can reproduce the tribological conditions that occurred in machining [4]. A wide variety of experiences are then needed to fully characterize the involved phenomena by reproducing the conditions of local pressure and sliding speeds. These conditions must be achieved with a simple geometry for which the measurement of the contact parameters can be made easily. In this paper, experimental results concerning the values of μ are presented. For characterizing the friction behaviour at the tool-chip interface, a mean normal pressure about 400 MPa and high sliding velocity are imposed during the presented tests. The extreme pressures (> 1 GPa) present near the tip-tool combined with low speed are not considered in the experimental study. An application in the case of FEM modelling of High Speed Machining is discussed.

2. EXPERIMENTAL DEVICES

An original sensor for measuring forces generated during friction is developed to combine high sliding speed and high contact pressure. This load sensor is integrated on a ballistic bench currently being tested at a maximum speed of 120 m/s. The ballistic device, presented in Fig. 1, is made up of two coaxial tubes. The first one is the launch tube and the second is the receiving tube leading to a shock absorber. This equipment was also developed for the study of cutting process under extreme conditions [5] and reproduce perfectly orthogonal cutting conditions without drawback induced by industrial machining. The quasi-instantaneous expansion of a compressed air propels a projectile at high speed into the launch tube. A sufficient length of this tube, combined with

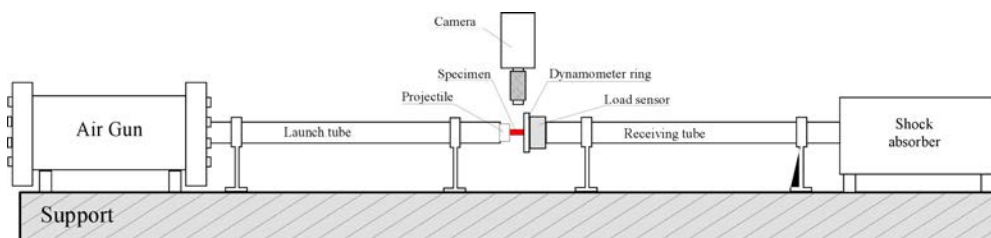


FIG. 1. Ballistic set-up dedicated to the cutting and the friction study.

a mass of the projectile adjusted (different geometries, different materials), provides almost constant speed (less than 4% variation) to the projectile during the process. A set of three sensors record precisely the velocity and acceleration of the projectile.

The load sensor schematically shown in Fig. 2a, attached to the receiving tube, supports a dynamometer ring that imposes a normal force (F_N) adjusted by the dimensions of the different part in contact. This force generates a normal pressure between the cutting tool and the specimen (moving specimen). Setting

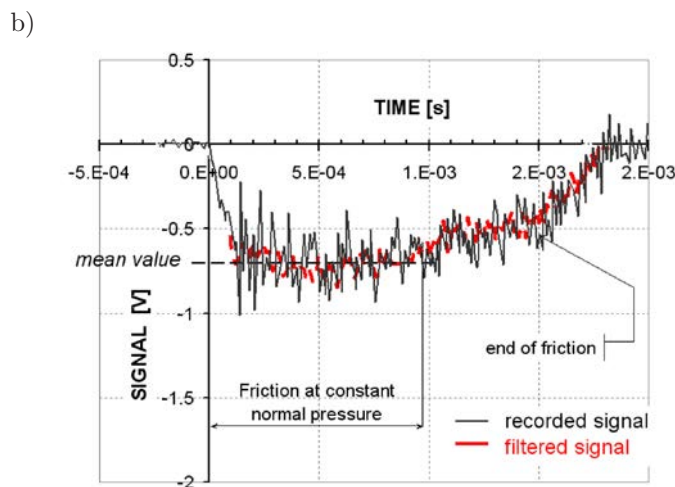
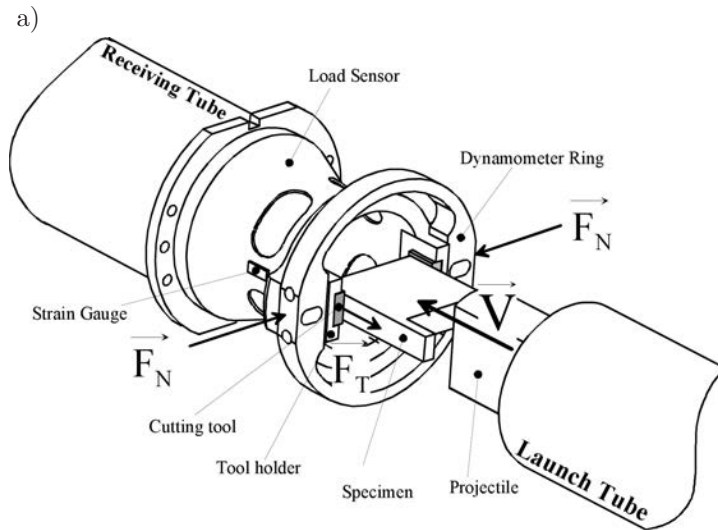


FIG. 2. a) Details of dynamical tribometer designed to able to reproduce the contact between a cutting tool and a workpiece; b) signal recorded by the strain gauge located on the load sensor at 40 m/s.

the translation speed of the specimen is caused by the impact of the projectile. The entire specimen is received in a shock absorber. The post-mortem analysis of rubbed surfaces is then possible. The load sensor was designed to be easily adapted to another propeller as a conventional dynamical hydraulic tensile machine. The hydraulic jack of the tensile machine takes the role of the projectile and ensures the movement of the specimen.

Figure 2b presents a recorded signal used to calculate the tangential force (F_T) and deduce the friction coefficient ($\mu = F_T/F_N$). The filtered signal is deduced from the signal recorded by the strain gauges by applying a LPF (low pass filter) of 10 kHz. The filtered signal significantly improves the visibility of a mean value of the friction force.

Experimental and numerical calibrations are performed to convert the mean signal value into force intensity. The load sensor and its implementation on the dynamic bench have been firstly modeled by FEM in ABAQUS. In a second part, it has been statically and dynamically calibrated, allowing the validation of the FEM model. This dynamic calibration has been achieved thanks to direct impacts of the projectile with different weights and for speeds limited at 10 m/s.

3. EXPERIMENTAL EVOLUTION OF THE FRICTION COEFFICIENT

Figure 3 illustrates the evolution of dry friction of a mid-hard steel C22 on an uncoated carbide tool. The steel friction surfaces are obtained by grinding in the same direction as the rubbing movement ($R_a = 0.8 \mu\text{m}$). It is important to note that the tests replicated friction conditions only with a single pass between two new surfaces (not running-in phase). It is observed that friction coefficient decreases with increasing sliding velocity according to previous works [6]. A similar trend has also been observed in [7, 8]. A minimum value of the coefficient seems to be reached and then with further increasing velocity an opposite tendency is observed.

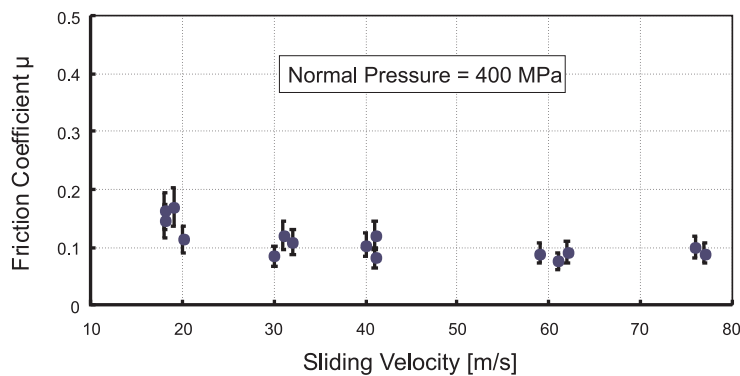


FIG. 3. Dry friction coefficient for the sliding of steel C22 on an uncoated carbide tool.

4. APPLICATION TO HSM

4.1. Modeling

The metal cutting is modeled by the finite element method thanks to the code ABAQUS/Explicit in version 6.8. The 2D model, with four nodes elements, follows a Lagrangian scheme to study the evolution of chip formation from its initial phase until the steady state. The tool is considered as an elastic rigid body while the workpiece material follows a thermoviscoplastic behavior described by the Johnson-Cook's law [9, 10]:

$$(4.1) \quad \bar{\sigma} = [A + B (\bar{\varepsilon}^p)^n] \left[1 + C \ln \left(\frac{\dot{\bar{\varepsilon}}^p}{\dot{\varepsilon}_0^p} \right) \right] \left[1 - \left(\frac{T - T_{\text{room}}}{T_{\text{melt}} - T_{\text{room}}} \right)^m \right],$$

where $\bar{\sigma}$ is the effective flow stress of the material, $\bar{\varepsilon}^p$ the effective plastic strain and $\dot{\bar{\varepsilon}}^p$ the effective strain rate, $\dot{\varepsilon}_0^p$ the reference plastic strain-rate of 1/s, T_{room} the room temperature and T_{melt} (1520°C) the melting temperature. A, B, C are the material constants, n the strain hardening exponent and m the thermal softening exponent.

Because of the similarity of compositions between the studied C22 steel and the CRS1018 steel, the other used parameters summarized in Table 1 are approximated by the results presented by [10, 11].

Table 1. Johnson-Cook parameters used for C22 steel.

A [MPa]	B [MPa]	N	C	m	D_1	d_2	d_3
520	269	0.282	0.0476	0.533	0.24	1.1	1.5

A damage criterion is also applied to the workpiece elements allowing the material separation [11, 12]. The failure of an element is effective when the critical the damage parameter D exceeds the value of 1:

$$(4.2) \quad D = \sum \frac{\Delta \bar{\varepsilon}^p}{\bar{\varepsilon}_f}.$$

$\Delta \bar{\varepsilon}^p$ is the increment of plastic deformation during a cycle of integration and $\bar{\varepsilon}_f$ the failure strain under the condition of triaxiality:

$$(4.3) \quad \bar{\varepsilon}_f = d_1 + d_2 \exp \left(d_3 \frac{\sigma_m}{\bar{\sigma}} \right),$$

where σ_m is the hydrostatic pressure and d_1 , d_2 and d_3 are the damage failure material constants reported in Table 1.

To calculate the friction stress, the following relationship is used:

$$(4.4) \quad \tau_f = \min(\mu p, \tau_{\text{crit}}).$$

At very high pressure, $\tau_f = \tau_{\text{crit}}$ where τ_{crit} is a maximum value that τ_f cannot exceed. For lower pressures, the friction Coulomb's law is then effective. The value of τ_{crit} is generally regarded as the shear flow stress k in the material. The choice of the parameters τ_{crit} and μ is critical because τ_{crit} and μp are also criteria to allow a contact element to slide along the tool. Therefore, these parameters control not only the values of the shear stress and the temperature rise but also the morphology of the chip.

4.2. Results and discussion

To study the influence of friction in the numerical model, cutting tests are carried in the same range of velocities. During these tests, the cutting force normal to the rake face is measured and used to emphasize the consequence of the friction parameter. Orthogonal cutting tests are performed on the same ballistic device [5] used for the friction tests. The load sensor is changed to support two symmetric carbide cutting tools. The workpiece is attached on the projectile. An intensified CCD camera is used to record temperature field during the process [13]. To carry out the numerical simulations, different approaches are conducted. In the first one, which is usually adopted, the value of τ_{crit} is constant and equal to the shear yield stress ($\tau_{\text{crit}} = k_0 = \sigma_0/\sqrt{3}$ with $\sigma_0 = 289$ MPa) and μ is fixed for all speeds. Two values of μ were firstly selected as 0.1 and 0.25. The range for μ was chosen from the experimental results illustrated in Fig. 3. Figure 4 shows the evolution of cutting forces as a function of cutting speed. Compared to the experimental results, the trends are conserved in spite of a certain overestimate for the cutting forces.

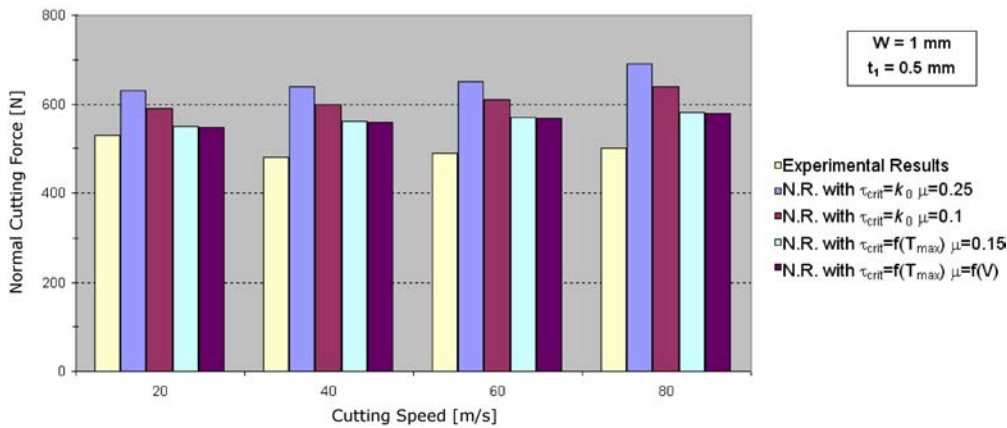
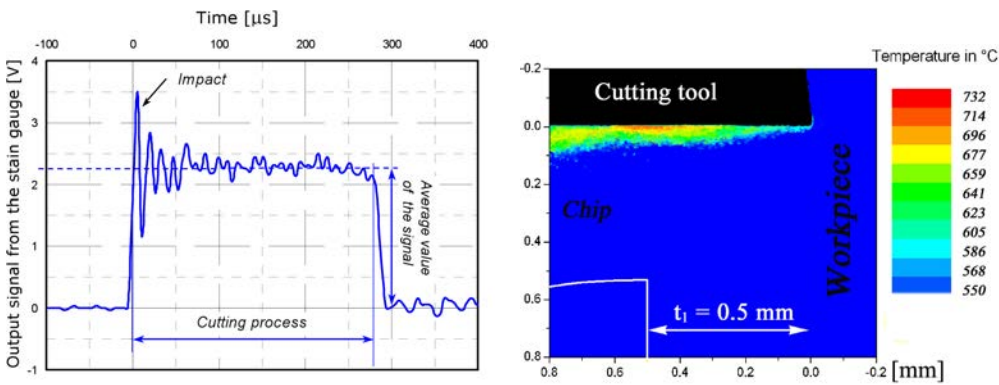


FIG. 4. Experimental and Numerical Results (N.R.) of the normal cutting force as a function of the cutting speed (C22).

A second approach can be performed, with a mean value of μ fixed to 0.15 and the critical stress defined as a function of the maximal contact temperature T_{\max} by Eq. (4.1): $\tau_{\text{crit}} = f(T_{\max})$. T_{\max} is deduced from the experimental temperature field measured in the chip during orthogonal cutting tests as shown in Fig. 5. This second approach is interesting because the numerical results are improved by trending to the experimental measurements. The cutting forces obtained in the simulations decrease due to the drop of τ_{crit} through the effect of thermal softening of the material. The last approach keeps τ_{crit} as a function of the temperature and adjusts the friction coefficient with the experimental values ($\mu = f(V)$), cf. Fig. 3. A weak difference of the results emphasizes that the role of μ is minimized in the friction stress modeling. Indeed, the combination of $\tau_{\text{crit}} = f(T_{\max})$ and $\mu = f(V)$ leads to $\tau_f = \tau_{\text{crit}} \leq \mu p$ over almost the entire contact area.

Figure 5 illustrates a comparison between the experimental and numerical results for the following cutting conditions: the rake angle $\alpha = 0^\circ$, the uncut chip

a)



b)

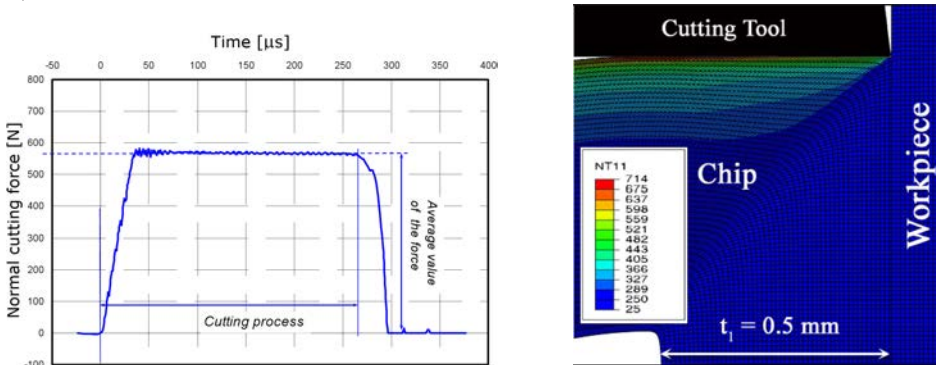


FIG. 5. Cutting forces and temperature maps obtained during orthogonal cutting test – material C22: a) experimental; b) simulation.

thickness $t_1 = 0.5$ mm and the cutting speed $V_C = 42$ m/s. A good correlation is observed not only for the cutting forces but also for the temperature field when the contact parameters are optimized.

5. CONCLUSION

The combination of three experimental devices allowed defining the friction coefficient for a large range of sliding velocities up to 80 m/s. The obtained values are applied to the high speed cutting process to describe the friction stress at the tool-chip interface. The equipment enables to reach the dry sliding friction condition with pressure of 400 MPa. Complementary orthogonal high cutting tests are also conducted in order to measure cutting forces and temperature fields in the chip. All experimental data are employed to validate the friction modeling in the finite element code ABAQUS. A good correlation is overall obtained. However, the results highlighted limits in the friction model based on Eq. (4.4) because the criterion restrict the effect of the contact temperature and the real friction coefficient μ . Coulomb's friction coefficient could be formulated according to the contact pressure, the temperature and the sliding velocity.

ACKNOWLEDGMENT

The material presented in this paper has been shown at Workshop 2012 on Dynamic Behavior of Materials and Safety of Structures, Poznan, 2–4 May, 2012.

REFERENCES

1. CHILDS T.H.C., MAHDI M., *On the stress distribution between the chip and tool during metal turning*, Annals of the CIRP, **38**, 55–58, 1989.
2. USUI E., SHIRAKASHI T., *Mechanics of machining – from descriptive to predictive theory*, ASME Publication PED, **7**, 13–35, 1982.
3. BURYRTA D., SOWERBY R. AND YELLOWLEY I., *Stress distribution on the rake face during orthogonal machining*, Int. J. Mach. Tools Manufacturing, **14**, 721–739, 1994.
4. BROCAIL J., WATREMEZ M., DUBAR L., *Identification of a friction model for modelling of orthogonal cutting*, Int. J. Tools and Manufacture, **50**, 807–814, 2010.
5. SUTTER G., *Chip geometries during high speed machining for orthogonal cutting conditions*, J. Mach. Tools Manufacturing, **45**, 719–726, 2005.
6. SUTTER G., PHILIPPON S., MOLINARI A., *An experimental investigation of dry friction for a large range of sliding velocities*, Matériaux et Techniques HS, pp. 33–37, 2004.
7. LIM S.C., ASHBY M.F., BRUNTON J.H., *The effects of sliding conditions on the dry friction of metals*, Metallurgica, **37**, 3, 767–772, 1989.

8. LIM S.C., ASHBY M.F., *Wear-Mechanism maps*, Acta Metallurgica, **35**, 1, 1–24, 1987.
9. JOHNSON G.R., COOK W.H., *A constitutive model and data for metals subjected to large strains, high strain rates and high temperatures*, Proc. 7th Inter. Symp. on Ballistics Proceedings, pp. 541–547, 1983.
10. SASSO M., NEWAZ G., AMODIO D., *Material characterization at high strain rate by Hopkinson bar tests and finite element optimisation*, Mat. Sci. Eng., **A487**, 289–300, 2008.
11. GOTO D., BECKER R., ORZECOWSKI T., SPRINGER H., SUNWOO A., SYN C., *Investigation of the fracture and fragmentation of explosively driven rings and cylinders*, Int. J. Impact Eng., **35**, 1547–1556, 2008.
12. JOHNSON G.R., COOK W.H., *Fracture characteristics of three metals subjected to various strains, strain rates, temperatures and pressures*, Eng. Fracture Mech., **1**, 31–48, 1985.
13. RANC N., PINA V., SUTTER G., PHILIPPON S., *Temperature measurement by visible pyrometry: orthogonal cutting application*, J. Heat. Transfer. ASME, **126**, 931–936, 2004.

Received April 14, 2012; revised version August 30, 2012.
